Application of the Random Pore Model to the Carbonation Cyclic Reaction

Gemma Grasa and Ramón Murillo
Instituto de Carboquímica (CSIC), Energy and Environmental Dept., C/Miguel Luesma Castán No. 4, 50015 Zaragoza, Spain

Mónica Alonso and J. Carlos Abanades
Instituto Nacional del Carbón (CSIC), Chemistry of Materials Dept., C/Francisco Pintado Fe, No. 26, 33011 Oviedo, Spain

DOI 10.1002/aic.11746
Published online April 7, 2009 in Wiley InterScience (www.interscience.wiley.com).

Calcium oxide has been proved to be a suitable sorbent for high temperature CO_2 capture processes based on the cyclic carbonation-calcination reaction. It is important to have reaction rate models that are able to describe the behavior of CaO particles with respect to the carbonation reaction. Fresh calcined lime is known to be a reactive solid toward carbonation, but the average sorbent particle in a CaO-based CO_2 capture system experiences many carbonation-calcination cycles and the reactivity changes with the number of cycles. This study applies the random pore model (RPM) to estimate the intrinsic rate parameters for the carbonation reaction and develops a simple model to calculate particle conversion with time as a function of the number of cycles, partial pressure of CO_2, and temperature. This version of the RPM model integrates knowledge obtained in earlier works on intrinsic carbonation rates, critical product layer thickness, and pore structure evolution in highly cycled particles. © 2009 American Institute of Chemical Engineers *AIChE J,* 55: 1246–1255, 2009
Keywords: CO_2 capture, regenerable sorbents, carbonation, kinetics, limestone

Introduction

The separation of a pure CO_2 stream, combined with a well-managed geological storage site is considered to be a major mitigation option for climate change.[1] The carbonation reaction serves as the basis for several high temperature CO_2 capture systems when it is coupled with a calcination step to produce a pure CO_2 stream. The use of the carbonation-calcination loop of $CaO/CaCO_3$ is now accepted as a viable technique for the capture of CO_2 in postcombustion[2–5] or in precombustion[6–10] routes. Figure 1 shows a possible scheme for the proposed CO_2 capture process for postcombustion application.[3] The system mainly consists of two interconnected circulating fluidized bed reactors: a carbonator and a regenerator or calciner. In the carbonator, the CO_2 present in the flue gas stream coming from a boiler meets a flux of CaO and reacts to form $CaCO_3$. In the calciner, a secondary fuel is fired with pure oxygen to supply the necessary heat to calcine the $CaCO_3$ formed in the carbonator and decompose it into CaO (which is returned to the carbonator) and CO_2, suitable for final purification, compression, and geological storage.

The design of the carbonator reactor requires a good understanding of the carbonation reaction rates of the CaO particles that enter the carbonator from the calciner. High reaction rates between the CO_2 in the flue gas and the sorbent particles are necessary to design absorbers of a reasonable size. Fresh calcined lime is known to be a very reactive solid in the carbonation reaction. However, the average sorbent particle must undergo many carbonation-calcination cycles[3] as a result of which sorbent capture capacity will decrease rapidly. Since the solids in both reactors in Figure 1 are assumed to be well mixed, the make up flow of limestone and the purge of CaO will result in a wide distribution of

Correspondence concerning this article should be addressed to G. Grasa gga@carbon.icb.csic.es

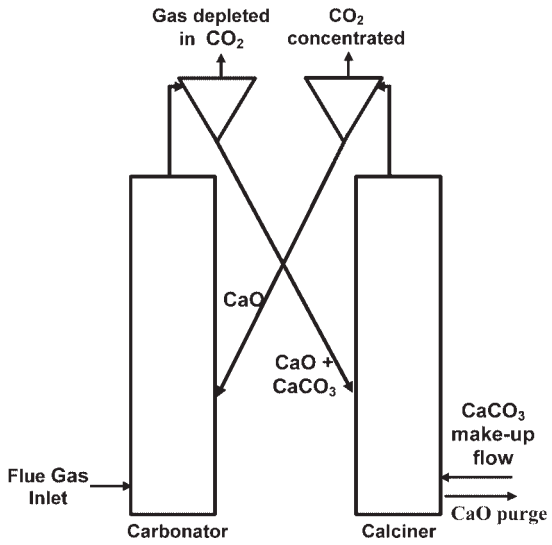

Figure 1. Schematics of the carbonation-calcination loop.

particle types in terms of cycle number and reactivity. Previous studies on the reversibility of the carbonation/calcination reaction have shown that carbonation is far from reversible in practice.[2,4,6,11–16] After a fast, chemically controlled initial reaction stage, a second slower reaction stage controlled by the diffusion in the product layer, $CaCO_3$,takes place.[13] It has also been observed that the transition between the fast and slow regimes takes place quite suddenly at a given level of conversion, and that this level of conversion decreases as the number of carbonation/calcination cycles increases. The evolution of the sorbent capture capacity of natural sorbents, with the number of cycles and varying process variables, has been studied in previous works.[14,15] It was found that this capacity decreases rapidly in the first 20 cycles but tends to stabilize at very high cycle numbers[15] at a residual conversion. Calcination temperatures over 950°C, and/or extended calcination times accelerate the degradation of the sorbent, which therefore attains the residual capture capacity with a lower number of cycles. Detailed observation by mercury porosimetry and SEM of the textural changes in limestone during cycling[14,16,17] led to the conclusion that the main mechanism of sorbent deactivation is the progressive sintering, or grain growth, of the originally rich texture resulting from the first calcination. According to this mechanism, after a certain number of cycles, the $CaCO_3$ formed during carbonation will occupy all the space in the small pores plus a small fraction of the large voids. However, the occupation of the large pores is limited by the thickness of the product layer that marks the onset of the slow carbonation period. Second-order effects (pore mouth blockage, isolated voids in the calcined particle, particle shrinkage) can also be detected in some special sorbents and conditions.[17] Essentially, though, it is the grain sintering mechanism as the number of cycles increases, and the thickness of the product layer in the large voids, that marks the decay of capture capacity.

Different descriptions of the carbonation reaction have been proposed through a gas–solid reaction model,[2,8,13,18,19] and a review of these carbonation models has been recently carried out by Stanmore and Gilot.[20] Among the models proposed are semiempirical models,[2,18] where the carbonation reaction is described by a simple rate expression based on the difference between the maximum carbonation conversion and the conversion at any point, multiplied by the kinetic constant and the average CO_2 concentration in the reaction atmosphere. Johnsen et al.[8] applied the shrinking core model to describe the carbonation reaction based on their SEM/EDS observations. They observed that the oxygen profiles in a partially carbonated particle displayed a nonuniform reaction pattern. The particle had an external rim indicating a high concentration of $CaCO_3$ and an inner core with a higher concentration in CaO. A third group of researchers applied pore models.[13,19] These pore models describe the carbonation reaction with greater accuracy as they take into account the evolution of pore size distribution during the cycling. Furthermore, many SEM studies of highly cycled samples suggest that a pore model may provide a better geometrical approximation for describing the texture of calcines. Adjusting the pore model to the grain model, with a suitable correction of the structural parameters, was established by Bhatia and Perlmutter as an effective procedure when they compared the grain model with their random pore model (RPM).[21,22] The RPM model considers the pore structure as a network of randomly interconnected pores, defines the particle structural parameters based on this geometry and finally, when it is applied to the carbonation reaction, provides kinetic parameters by fitting the experimental reaction rate data obtained from "fresh lime"[13] (only one calcination). Recently, a new gas–solid model based on discrete pore size distribution measurements was developed by Sun et al.[19] This model uses the initial pore size distribution of the calcine as input data, the only fitting parameter being the effective diffusivity in the product layer (which is also dependent on the evolution of the pore system). The same group determined intrinsic kinetic constants in a previous work and they included them in the model equations.[23] The results obtained from the application of their model are in agreement with experimental data over a wide range of temperatures and partial pressures of CO_2. However, this model is difficult to apply because it requires as input data the initial pore size distribution after calcination. Until now this model has only been applied to "fresh lime."

The need for reaction rate models to the carbonation of highly cycled CaO particles is relatively new procedure and related to the development of carbonate looping processes for CO_2 capture. In a previous work by our group,[24] a simple homogenous model was applied to describe the carbonation reaction during the fast reaction period of highly cycled particles of CaO. In these conditions, all resistance to chemical reaction was eliminated due to the distribution of wide pores resulting from multiple carbonation/calcination.[16,17] A simplified homogeneous reaction model was found to be sufficient for describing the carbonation reaction of highly deactivated particles.

We have attempted in this work to derive a carbonation reaction model valid for any number of cycles and able to represent CaO conversion with time as a function of the cycle number and carbonation reaction conditions (temperature, CO_2 partial pressure). To achieve this objective, the following experimental work was carried out in order to obtain information about the reactivity of different types of lime particles toward carbonation.

Experimental

The cyclic carbonation and calcination reactions were experimentally studied in a thermogravimetric analyzer (TGA) specially designed to derive reactivity data during carbonation in long multicycle carbonation-calcination tests. The TGA, consisted of a quartz tube placed inside a two-zone furnace capable of working at temperatures up to 1000°C. The temperature and sample weight were continuously recorded on a computer. The reacting gas mixture (CO_2, O_2/air) was regulated by mass flow controllers and fed into the bottom of the quartz tube. A special characteristic of this TGA is the presence of two zones in the furnace capable of working at different temperatures. The furnace can be moved up and down by means of a pneumatic piston. Its position with respect to the platinum basket alternates between calcination conditions (>850°C) or carbonation conditions (around 650°C). For each run in the TGA around 2 mg of sorbent was introduced in the sample holder to avoid interparticle diffusion effects in the platinum basket. Preliminary experiments were carried out to determine the total gas flow needed to eliminate external diffusion effects around the sample basket (this was finally set to 4×10^{-6} m^3/s, i.e., about 0.06 m/s of superficial gas velocity around the sample basket at 650°C and 0.08 m/s at 950°C). Preliminary experiments were performed using an empty sample holder and an inert material to determine the effect of disturbances on the weight readings when the furnace is moved from the calcination to the carbonation position (a rapid change in temperature modifies the gas velocity around the sample basket). After correcting the data obtained from the preliminary blank tests, CaO conversion vs. time for each cycle was calculated by measuring the weight losses and assuming that the CaO was converted to $CaCO_3$ during carbonation. At the end of each run, the samples were weighed in a different balance to check the accuracy of the TGA experiment. Good agreement was found in all cases between the overall conversion calculated from this final weight difference and the TGA conversion. Although the TGA has been designed to allow for fast changes in temperature around the sample holder, there is still a delay in the order of 30–60 s before the desired carbonation temperature is reached after the calcination step. To stop the carbonation reaction during this temperature stabilization period, the flow of CO_2 was switched off until the carbonation temperature was stable within a ±5 K difference with respect to the preset temperature. Two different limestones were used during the experiments (a Spanish limestone called Imeco and a Polish limestone called Katowice). A series of test was carried out to determine the effect of particle size on the carbonation rate experiments. Three particle size cuts were tested: 50–75 μm, 100–300 μm, and 300–600 μm. However, since the main objective of this work was to derive intrinsic carbonation rates, a narrow particle size cut was used (50–75 μm) for both limestones in most tests. Both limestones were characterized by using a Hg Porosimeter Quantachrome PoreMaster to determine their structural parameters according to the RPM. The carbonation reaction was studied over the range of 550 to 750°C and the pCO_2 was varied between 0.01 and 0.1 MPa.

Results

Figure 2 shows typical curves representing CaO conversion, X, vs. time for different carbonation temperatures and for both limestones (weight changes were measured every second). The curves represent key features described in other published works related with the carbonation reaction.[2,6,11–20,23,24] After a fast initial reaction controlled by chemical reaction (kinetic regime), there is an abrupt change in the carbonation reaction rate. This change to a second slower stage has been attributed to the mechanism of CO_2 diffusion through a $CaCO_3$ layer that starts to control the reaction at this point.[13,16,19]

Alvarez and Abanades[16] concluded that the thickness of the product layer was a critical parameter for understanding the carbonation reaction during the fast and slow reaction periods and the transition between these two differentiated reaction rates. By means of mercury porosimetry they observed that, for several limestone types and for a different number of carbonation/calcination cycles, a carbonate layer of 49 nm formed on the available CaO surface and that this was responsible for the end of the fast reaction period. However, characterization of this critical parameter does not provide sufficient information to ensure the correct design of the carbonator reactor. It is also necessary to establish the correct carbonation rates before the formation of this critical

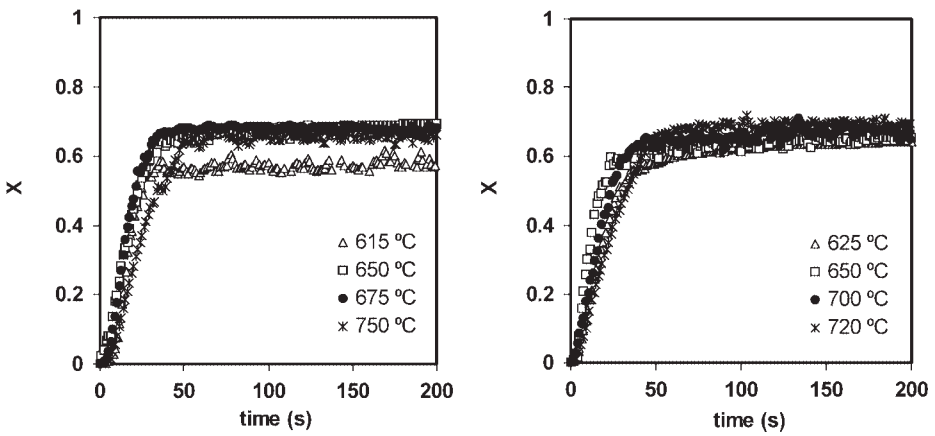

Figure 2. CaO conversion curves for different carbonation temperatures.

(Left) Imeco limestone. (Right) Katowice limestone. Calcination in air at 900°C, 10 min: pCO_2 during Carbonation 0.01 Mpa.

Table 1. Characteristics of the Calcines from the Limestones Tested in This Work and Structural Parameters

Limestone	S_o (m^2/m^3)	L_o (m/m^3)	ε	Ψ	k_{so} (m^4/kmols)	E_{aK} (kJ/kmol)	D_o (m^2/s)	E_{aD} (kJ/kmol)
Imeco	42×10^6	4.16×10^{14}	0.47	1.52	0.559×10^{-5}	21.3×10^3	3.37×10^{-6}	163×10^3
Katowice	35×10^6	2.63×10^{14}	0.46	1.41	0.529×10^{-5}	19.2×10^3	4.32×10^{-6}	163×10^3

Kinetic and diffusion parameters defined further on in the article are also included in this table.

product layer. The carbonation reaction rate before the formation of the critical product layer will probably have a component of an intrinsic kinetic nature and a component associated to the diffusivity of CO_2 through the growing carbonate layer until the small pores are filled up to the critical value of ~50 nm, after which diffusivity tends to be very low. This last point is consistent with the findings of Mess et al.[25] who found that CO_2 diffusivity in the carbonate product layer decreased rapidly with increasing carbonate conversion. Therefore, our first application of the RPM model to the experimental results was aimed at determining the intrinsic parameters characteristic of a reaction regime somewhere in between the two extremes described earlier: kinetic control for low carbonation conversions and increasing importance of diffusion control as the product layer of $CaCO_3$ builds up. In fact, the RPM has already been developed and applied in the past for this purpose, and for other gas–solid reactions[13,21,22,26] and so only needed to be adapted to the special characteristics of the calcines obtained from the multiple calcination-carbonation cycles.

Bathia and Perlmutter developed a general expression for the instantaneous solid–gas local reaction rate applicable to porous systems in the presence of product layer diffusion resistance:

$$\frac{dX}{dt} = \frac{k_s S_o C (1-X)\sqrt{1-\Psi \ln(1-X)}}{(1-\varepsilon)\left[1+\frac{\beta Z}{\Psi}\left(\sqrt{1-\Psi \ln(1-X)}-1\right)\right]} \quad (1)$$

This expression correlates particle conversion, X, with the internal solid pore structure by defining the structural parameter Ψ, which accounts for this internal particle pore structure in terms of:

$$\Psi = \frac{4\pi L_o (1-\varepsilon)}{S_o^2} \quad (2)$$

where L_o represents the initial total pore length in the porous system per unit of volume; S_o the initial surface area per unit of volume and ε the porosity. L_o, S_o, and ε can be directly calculated from the mercury porosimetry data[26] as follows:

$$S_o = 2\int_0^\infty \frac{\upsilon_o(r)}{r} dr \quad (3)$$

$$L_o = \int_0^\infty \frac{\upsilon_o(r)}{\pi r^2} dr \quad (4)$$

and

$$\varepsilon = \int_0^\infty \upsilon_o(r) dr \quad (5)$$

Mercury porosimetry was applied to fresh calcines of both limestones in order to determine these parameters. The results are compiled in Table 1 together with the structural parameter Ψ. Figure 3 shows the pore size distribution for the first calcines of both limestones. They both present a unimodal pore distribution although the Katowice limestone shows a wider pore distribution. The Imeco limestone has a mean pore diameter of 35 nm, whereas the Katowice limestone presents a mean pore diameter of ~50 nm.

The carbonation reaction was found to be first order with respect to the CO_2 concentration up to pCO_2 0.1 MPa[2,13,24,27] (see also Figure 4). This is in contrast with the results of Sun et al.[23] who considered the reaction to be first order up to 0.01 MPa and zero order for higher CO_2 partial pressures.

Radial diffusion resistances through the pore network of the particle were neglected in our application of the RPM model to the experimental data. Carbonation tests conducted with different particle size (Figure 5) up to what can be reasonable particle size of these materials when used in similar circulating fluidized beds combustors (typically lower than 300 μm) shows that its effect is modest on reaction rates. Furthermore, Figure 5 shows that the effects are almost negligible after the fourth carbonation cycle. Since the application of carbonate looping cycles in postcombustion processes will require operation with fine and highly cycled materials in CFBs, we have focused the application of the RPM model on the 50–75 μm size cut.

For a reversible first-order system, the general rate expression from Eq. 1 can be simplified and integrated in the regime of chemical reaction control, and therefore the particle conversion is given by:

$$\frac{1}{\Psi}\left[\sqrt{1-\Psi \ln(1-X)}-1\right] = \frac{k_s S_o (C_b - C_e) t}{2(1-\varepsilon)} \quad (6)$$

This expression was used to derive intrinsic kinetic constants for the carbonation reaction. To obtain reliable parameters

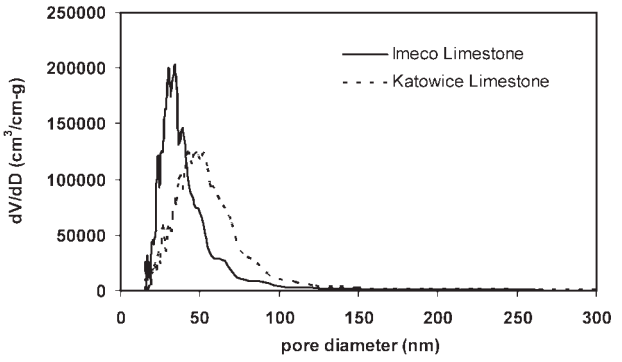

Figure 3. Pore size distribution for both limestones tested.

Calcination at 900°C in air.

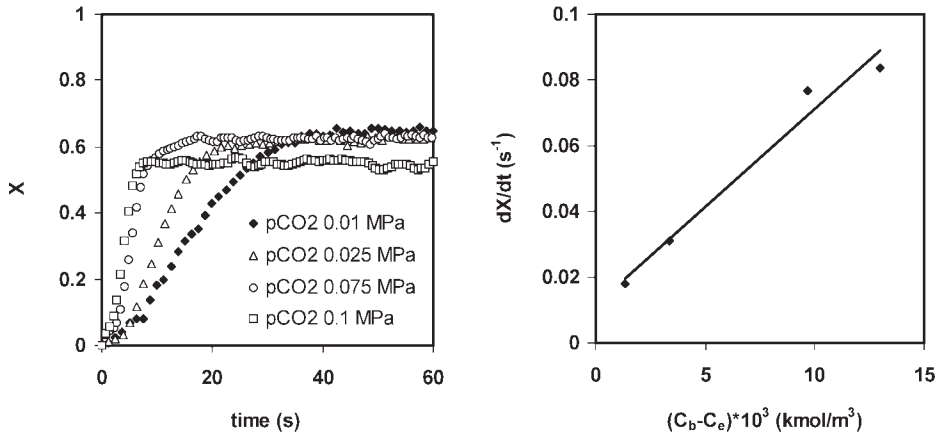

Figure 4. (Left) Experimental carbonation curves for different CO_2 partial pressures; carbonation temperatures 650°C, Imeco limestone; (right) mean delta conversion with time for different CO_2 partial pressures.

from this fitting exercise, it was important to ensure that external diffusion resistances were eliminated (by adjusting the thermo balance to allow a sufficient gas flow around the sample basket, and using a small amount of sample as indicated in the Experimental section). Figure 6 shows a sample of the results, from which the left hand side in Eq. 6 has been plotted against time. Therefore from the initial part of the slope in Figure 6, k_s for each experiment can be calculated.

An Arrhenius representation was plotted for individual values of k_s obtained from the conversion curves at different temperatures. From the slope and the ordinate in the origin, k_{so} (m^4/kmols) and E_{aK} (kJ/kmol) were determined for both sorbents.

$$k_s = k_{so}\exp(-E_{aK}/RT); k_s(\mathrm{m}^4/\mathrm{kmols}) \tag{7}$$

The values of k_{so} and E_{aK} have been included in Table 1 for both limestones tested. The mean activation energy for the carbonation reaction, $(20.3\pm 1.0)\times 10^3$ kJ/kmol, is in close agreement with the values found by Sun et al., $(29\pm 4)\times 10^3$ kJ/kmol for limestones, and fairly consistent with the values extracted from the equilibrium data,[23] although there are discrepancies with the values presented by Dennis and Hayhurst[27] and Bhatia and Perlmutter,[13] who reported that the carbonation reaction had zero activation energy in the kinetically controlled region. However, the k_s values obtained in the range of temperatures tested fall within the range of values reported by these authors (mean value of 0.05×10^{-5} m^4/kmols against the 0.06×10^{-5} m^4/kmols obtained by Bhatia and Perlmutter for the same range of temperatures).

Within the limit of product layer diffusion control, k_s/D_p tends to infinity and Eq. 1 can be integrated to the limiting form:

$$\frac{1}{\Psi}\left[\sqrt{1-\Psi\ln(1-X)}-1\right]=\frac{S_o}{(1-\varepsilon)}\sqrt{\frac{D_p t}{2Z}} \tag{8}$$

D_p being the apparent product layer diffusion coefficient. This can be estimated representing the left hand side in Eq. 8 vs. the root of time, as shown in Figure 7. This parameter is

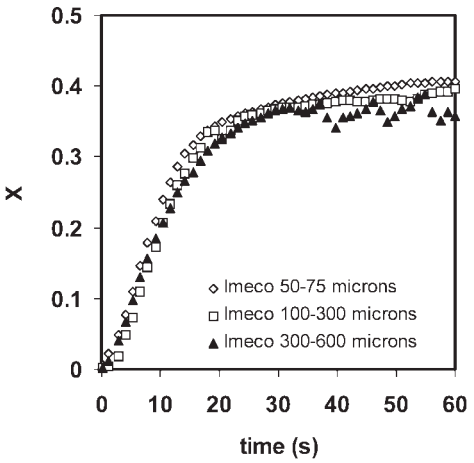

Figure 5. Experimental carbonation curves for different particle sizes.

Fourth carbonation cycle; Carbonation temperature 650 °C, pCO_2 0.01 MPa.

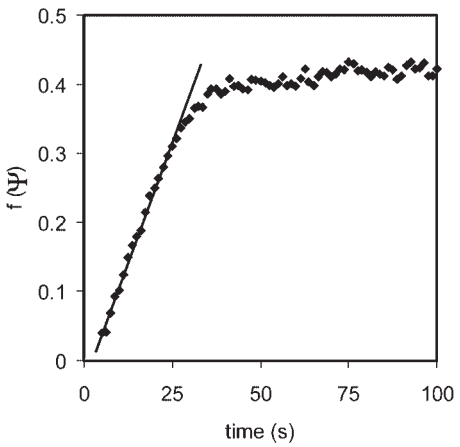

Figure 6. Representation of f(Ψ) vs. time for an individual curve from Figure 2.

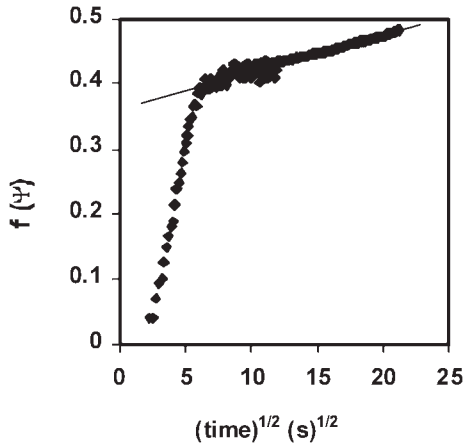

Figure 7. Representation of f(Ψ) vs. the root of time for an individual curve from Figure 2.

also related to the effective diffusion coefficient, D, as follows:

$$D_p = \frac{bM_{CaO}DC}{a\rho} \tag{9}$$

From the slopes in each figure (see Figure 7), the apparent diffusion coefficient, D_p, and therefore the effective product layer diffusion coefficient, D, have been estimated. This parameter can also be represented in an Arrhenius equation[13]:

$$D = D_o \exp(-E_{aD}/RT);\ \text{with}\, D(m^2/s) \tag{10}$$

The values for D_o and E_{aD} are compiled in Table 1 and the mean activation energy, E_{aD} $(163 \pm 15) \times 10^3$ kJ/kmol, is in close agreement with the values reported by Bhatia and Pelmutter[13] and compiled by Mess et al.[25] (178×10^3 kJ/kmol for temperatures above 515°C).

At this point, the intrinsic parameters k_s and D_p, for the carbonation reaction were determined and the carbonation conversion with time can be calculated using the RPM models (Eq. 1). However, we found that if the product layer diffusion resistance is calculated from the very beginning of the reaction much lower CaO conversions than experimental ones are obtained (despite the low thickness of the product layer at low carbonation conversions). Furthermore, the abrupt change in conversion rate that is apparent in the experimental plots of conversion vs. time (see for example Figure 2) is not sufficiently well reflected by the RPM model when diffusion coefficients lower than those compiled in Table 1 are taken into consideration in order to model the diffusion resistance at low carbonation conversions. It is therefore more practical to distinguish two reaction periods in the model: a first period where diffusion through the growing product layer is totally neglected (kinetic control only, the progress of reaction is governed by Eq. 14) and a second period where diffusion resistance is added to kinetic resistance (Eq. 16). The change in reaction rate between these two periods can be justified via two mechanisms: the effect of a variable product layer diffusion resistance that increases, as the product layer thickness increases (this was confirmed in the case of Mess et al.[25] for thick product layers) or alternatively, the initial formation of $CaCO_3$ islands on the free surface of CaO which grow until the individual $CaCO_3$ grains coalesce to form a $CaCO_3$ product layer that is able to seal the free CaO surface. In both mechanisms, there is reason to believe that diffusion reaction control starts to take effect (through the effective CO_2 diffusivity of Eq. 10) only after a certain level of product layer thickness has been reached. In both mechanisms, CO_2 diffusion is very fast and does not affect the progress of carbonation for low conversions (low product layer thickness). From a practical point of view, both mechanisms can be simplified and represented in the same form: an initial reaction stage controlled by the kinetic constant and a second stage where both the diffusion coefficient and kinetic constant control the progress of the carbonation reaction.

In the following paragraphs we will try to define the threshold that divides the two reaction regimes. Some published works (Sun et al.[23]) have limited the kinetic control to the initial stages of reaction (only up to a very low carbonation conversion). However, our experimental data show that the fast stage of the carbonation reaction follows an almost linear slope up to a CaO molar conversion of around 0.5–0.6 for a "fresh" calcined sample, when the maximum carbonation conversion is around 0.7. Therefore, the threshold between kinetic control and kinetic and diffusion control must be higher.

To determine this threshold between kinetic control and combined product layer diffusion and kinetic control, we resort again to the pore geometry distribution implicit in the RPM model, which was used earlier by Alvarez and Abanades[16] to calculate the product layer thickness at the end of the fast carbonation reaction (which included both the kinetic period and the period of transition to a very low reaction rate controlled only by diffusion). According to this model, for a given pore size distribution, the evolution of particle conversion with the product layer thickness can be estimated from Eq. 11:

$$X = \frac{M_{CaO}}{V^M_{CaCO_3}} \sum_i \left[\left(\frac{R_i + h_i - \delta_i}{R_i} \right)^2 - \left(\frac{R_i - \delta_i}{R_i} \right)^2 \right] \Delta V_i^{cum} \tag{11}$$

where ΔV^{cum} is the delta volume from direct Hg mercury porosimetry, R_i is the pore radius for every pore interval, δ_i corresponds to the decrease in pore radius upon carbonation, and h_i is the product layer thickness at every pore interval. The decrease in pore radius during carbonation was estimated from geometrical considerations and can be related to pore radius, product layer thickness, and α, according to:

$$\delta_i = h\alpha + R_i - \sqrt{h^2\alpha^2 + R_i^2 - \alpha h^2} \tag{12}$$

The parameter α corresponds to the volume fraction of carbonate invading the former volume of pore i, and can be calculated from the molar volumes of CaO (16.9×10^{-3} m^3/kmol) and $CaCO_3$ (36.9×10^{-3} m^3/kmol) according to:

$$\alpha = \frac{V^M_{CaCO_3} - V^M_{CaO}}{V^M_{CaCO_3}} = 0.54 \tag{13}$$

When the small pores are filled up, the product layer thickness becomes: $h_i = \min\left(\sqrt{\frac{1}{\alpha}}R_i, h_L\right)$; h_L being the critical product layer thickness found in Alvarez and Abanades[16] (49 nm).

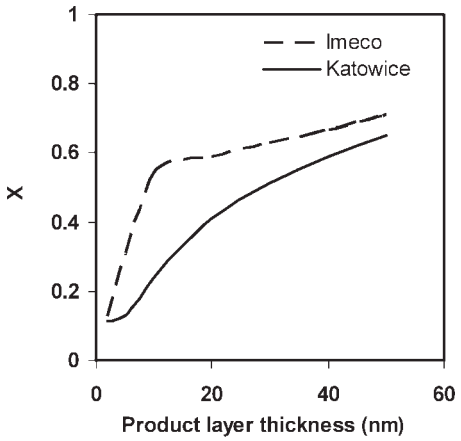

Figure 8. Evolution of particle conversion with the growth of product layer thickness on pore size distribution from Figure 3.

If this model is applied to the pore distributions from Figure 3, the CaO conversion from this point can be obtained for different product layer thicknesses. The results are plotted in Figure 8. It can be seen from Figure 3 that the mean pore diameter for the Imeco limestone is 35 nm, and that it presents a narrow pore size distribution. Therefore, by applying Eqs. 11–13 it can be observed in Figure 8 that CaO conversion rapidly increases while the smaller pores are being filled and that later the product layer continues to grow in the bigger pores until it reaches the limit of 49 nm established in the previous work cited earlier.[16] The Katowice limestone mean pore diameter is 50 nm, and its pore size distribution is wider than for Imeco limestone. Therefore, when the pore model developed by Alvarez and Abanades is applied, the CaO conversion curve and also the transition between the filling of the small pores and the larger ones is more gradual. According to the experimental conversion curves represented in Figure 2 and the relation between the product layer and particle conversion (Eq. 11), a mean product layer thickness of between 30 and 40 nm is determined as the borderline between kinetic and combined kinetic and diffusional control.

In the light of the previous analysis, the application of the RPM to the carbonation reaction was carried out as follows:

Assuming that a chemically controlled reaction stage governs the CaO conversion (up to a product layer of 30–40 nm), Eq. 14 was applied to calculate the CaO conversion as a function of time thus:

$$X = 1 - \exp\left(\frac{1 - \left(\frac{\tau}{2}\Psi + 1\right)^2}{\Psi}\right) \tag{14}$$

where

$$\tau = \frac{k_s(C_b - C_e)S_o t}{(1-\varepsilon)} \tag{15}$$

When the product layer thickness reaches 30–40 nm, and the particle conversion is around 0.55–0.6 for the first cycle (this value of conversion corresponding to the transition between regimes will be named $X_{K\text{-}D}$), diffusion resistance increases and both the diffusion coefficient and kinetic constant control

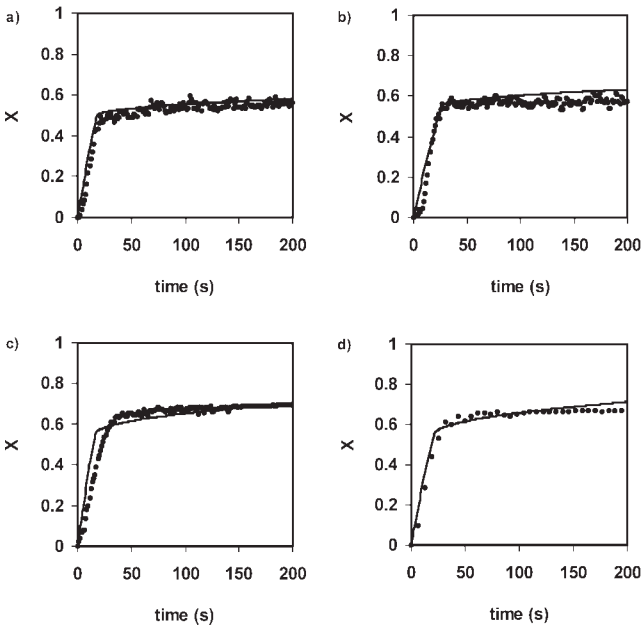

Figure 9. Experimental conversion curves and those predicted by the RPM for Imeco Limestone.

Carbonation temperature: (a) 550 °C; (b) 615 °C; (c) 650 °C and (d) 715 °C. pCO_2 during carbonation 0.01 MPa. Reaction and structural parameters from Table 1.

the carbonation reaction. The CaO conversion from this point can then be calculated from Eq. 16.

$$X = X_{k-D} + \left(1 - \exp\frac{1}{\Psi} - \frac{\left[\sqrt{1+\beta Z\tau} - \left(1 - \frac{\beta Z}{\Psi}\right)\right]^2 \Psi}{\beta^2 Z^2}\right) \tag{16}$$

$$\beta = \frac{2k_s a\rho(1-\varepsilon)}{M_{CaO} b D_p S_o} \tag{17}$$

Figures 9 and 10 show the results obtained from the application of Eqs. 14–17 using the structural, kinetic, and

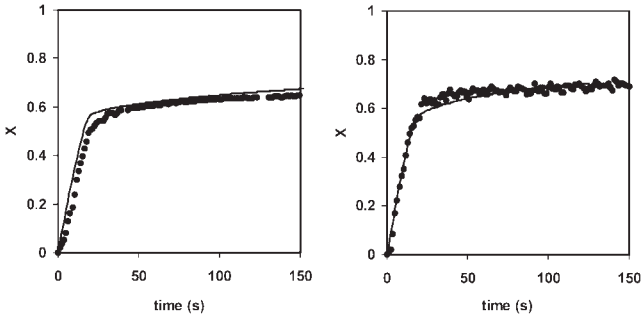

Figure 10. Experimental conversion curves and those predicted by the RPM for Katowice Limestone.

Carbonation temperature: (left) 600 °C; (right) 650 °C. pCO_2 during carbonation 0.01 MPa. Reaction and structural parameters from Table 1.

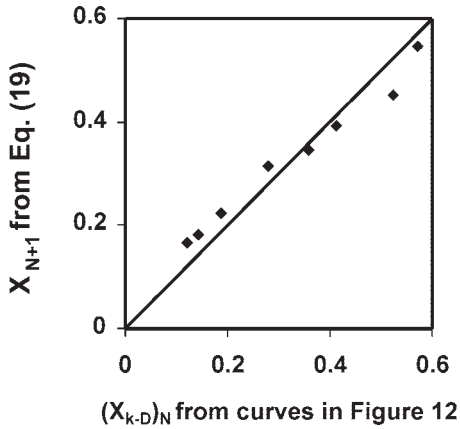

Figure 11. Experimental $X_{k\text{-}D}$ from Figure 12 vs. X_{N+1} from Eq. 19 for Imeco limestone.

diffusional parameters from Table 1. As can be seen, the results reflect fairly well the experimental results for the range of temperatures tested and for the timescale considered suitable for the CO_2 capture process proposed. Similar curves were plotted for the Katowice limestone.

At this point, the RPM has been successfully applied to describe the carbonation of the CaO particles resulting from one calcination. However, it is well known that the sorbent texture evolves with the number of carbonation/calcination cycles and that the slow carbonation period begins at a lower CaO conversion. Because of repetitive carbonation/calcination cycles, the initial rich texture of the fresh calcines evolves to a larger pore size distribution, and these results in a loss of surface for the reaction. To apply the model described in this work to a multicycle carbonation process, it is necessary to assume that the $CaCO_3$ product layer on which the change of reaction mechanism takes place (from kinetic to kinetic plus diffusion control) is similar to the one obtained in the previous paragraphs for the first cycle. Ideally we should know the pore size distribution after every calcination (to obtain S_N and L_N as in Eqs. 3 and 4) and apply the model described through Eqs. 11–13. But this would require a detailed sintering model to be able to estimate the pore size distribution during cycling. Although no such model exists, on the basis of the knowledge acquired on the evolution of the carbonation reaction with the number of cycles and the textural evolution of the sorbent, a series of simplifications can be performed[14–17] to calculate the structural parameter of the sorbent with the number of cycles and $(X_{K\text{-}D})_N$. Since large pore diameters (200–800 nm) are typical of highly cycled samples, it can be assumed that the $CaCO_3$ forms a layer (up to the limit of thickness h_L, ~49 nm) on the reaction surface S_N (m^2/m^3) which can therefore be estimated as follows for highly cycled particles of large pores (pore diameters [dmt] 50 nm)[24]

$$S_N = S_o X_N (m^2/m^3) \tag{18}$$

where X_N is the maximum carbonation conversion that the CaO particles achieve during the cycle number, N.

$$X_N = \frac{1}{\frac{1}{(1-X_r)} + kN} + X_r \tag{19}$$

For a large number of limestones and carbonation and calcination conditions,[15] X_r was found to be equal to 0.075 and k to be equal to 0.52. Assuming that the total pore volume will remain almost constant with the number of calcinations and that the pore diameter increases in size up to 1000 nm for highly cycled particles, L_N can be estimated thus:

$$L_N = L_o X_N \frac{rp_o}{rp_N} (m/m^3) \; rp_o/rp_N \approx 1 \text{for the initial cycles;}$$
$$rp_o/rp_N \approx 0.1 \text{for highly cycled particles} \tag{20}$$

It can be experimentally observed (see Figures 12 and 13) that there is still an abrupt change in reaction rate at a given CaO conversion (named $X_{K\text{-}D}$ in this work) for highly cycled samples, whose value decreases with the number of cycles. This conversion at which the transition between kinetic and combined diffusion takes place, must also be related to the mean product layer ($h_{K\text{-}D}$):

$$(X_{K-D})_N = \frac{S_N M_{CaO} h_{K-D}}{V^M_{CaCO_3} \rho_{CaO}} \tag{21}$$

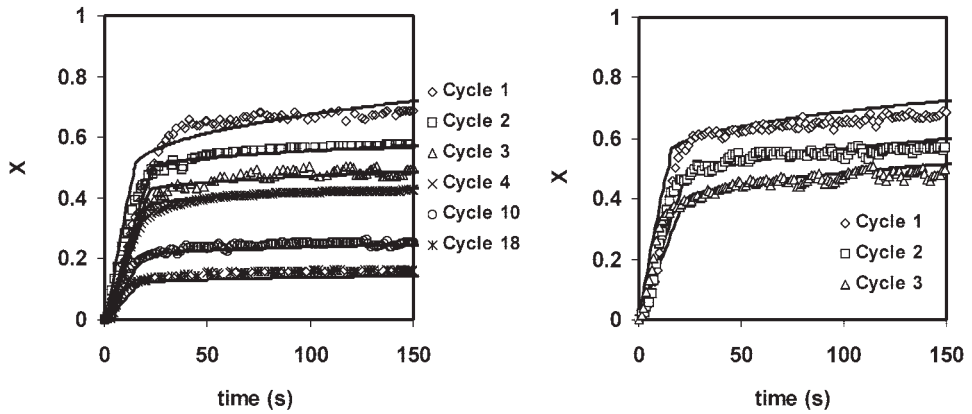

Figure 12. Experimental conversion curves and those predicted by the RPM for Imeco limestone (left), and Katowice limestone (right) for different cycle number.

Carbonation temperature 650°C, pCO_2 during carbonation 0.01 MPa. Reaction parameters from Table 1.

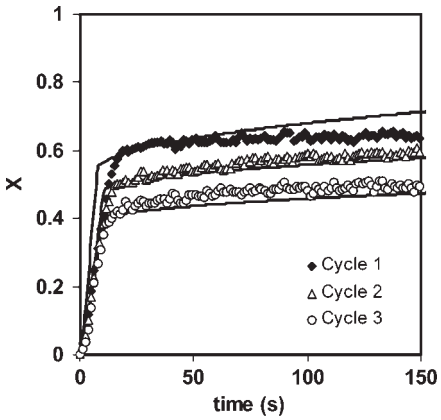

Figure 13. Experimental conversion curves and those predicted by the RPM for Imeco limestone applied for different cycle numbers. pCO_2 during carbonation 0.025 MPa.

Carbonation temperature: 640 °C. Reaction parameters from Table 1.

Using the experimental $X_{K\text{-}D}$ values from the individual curves in Figures 9 and 10, values of product layer thickness ranging from 30 to 42 nm were found to determine the change in reaction mechanism ($h_{K\text{-}D}$). From these results, and for a practical application of the model, a mean value of 38 nm is proposed as the threshold between kinetic and combined kinetic plus diffusional control for any given cycle.

It has also been experimentally observed that $X_{K\text{-}D}$ for a given cycle N is in close agreement with the maximum capture capacity X for cycle $N + 1$ calculated through Eq. 19. As can be seen in Figure 11, $(X_{K\text{-}D})_{N,\text{experimental}} \approx (X)_{N+1}$ from Eq. 19. It is not yet clear if this is a relevant observation for understanding the sintering mechanism during the carbonation-calcination cycles, but in the absence of better information this rule could be applied to estimate $X_{K\text{-}D}$ for other limestones and conditions that produce deactivation curves different to those used in this work.

Once S_N, L_N (and therefore Ψ_N), and $X_{K\text{-}D}$ have been estimated for every cycle, Eqs. 14–17 can be applied to calculate particle conversion against time. Figure 12 shows the results obtained with the carbonation model for different numbers of cycles and for both limestones tested.

The model described earlier has also been applied to obtain conversion curves vs. time for experiments carried out with the Imeco limestone, for carbonation $T = 650$°C and $pCO_2 = 0.025$ MPa in air. Figure 13 shows the evolution of the carbonation reaction after three successive calcination-carbonation cycles.

As can be seen from the previous figures, the RPM model proposed here is capable of fitting with a reasonably good accuracy the carbonation rates obtained in the relevant range of reaction times and conditions for the carbonate looping concept to be successfully applied.

Conclusions

The RPM has been applied in this study to estimate the intrinsic kinetic and diffusion parameters for the carbonation reaction in CaO particles that have experienced one or more calcination-carbonation cycles. The values for the parameters estimated are in close agreement with values found in the literature for carbonation after one calcination. The carbonation reaction can be successfully described as a two stage reaction. In the first stage, the carbonation is controlled by chemical reaction and in the second period there is a combined control by chemical reaction and CO_2 diffusion through the product layer. The RPM can be applied to determine the thickness of the product layer that marks the change in the reaction mechanism. This change was found to be around 30–42 nm for the limestones tested for different conditions and cycle numbers, with a mean value of 38 nm. Below this product layer thickness the particles react following a chemically controlled, first-order reaction, with an activation energy of 21.3×10^3 kJ/kmol for the Imeco, and 19.2×10^3 kJ/kmol for the Katowice limestone. The pre-exponential factors were 0.559×10^{-5} and 0.529×10^{-5} m^4/kmols, respectively. At higher conversions, the additional resistances associated with the CO_2 diffusion mechanism (mean activation energy, E_{aD} being 163×10^3 kJ/kmol; and the pre-exponential factors D_o being 3.37×10^{-6} and 4.32×10^{-6} m^2/s for Imeco and Katowice, respectively) must be allowed to obtain a good quality fit of the experimental kinetic data obtained in the relevant range of reaction times and conditions for the practical application of the carbonate looping concept.

Acknowledgements

This work is partially funded by the European Commission (C3-Capture) and the Spanish Ministry of Education ("Juan de la Cierva" program).

Notation

a, b = stoichiometric coefficients for carbonation reaction
C = concentration of CO_2, kmol/m^3; b, bulk concentration; e, equilibrium
D = effective product layer diffusivity, m^2/s
D_o = pre-exponential factor in Eq. 10, m^2/s
D_p = $bM_{CaO}DC/a\rho$ apparent product layer diffusion, m^2/s
E_{aK} = activation energy for the kinetic regime, K, kJ/kmol
E_{aD} = activation energy for the combined diffusion and kinetic regime, D, kJ/kmol
$h_{L,\ K\text{-}D}$ = product layer thickness, m; L, limiting product layer thickness; K-D transition between reaction regimes
k_{so} = pre-exponential factor in Eq. 7, m^4/kmols
k_s = rate constant for surface reaction, m^4/kmols
$L_{o,\ N}$ = initial total length of pore system, m/m^3; N, pore length for cycle N
M_{CaO} = molecular weight of CaO, kg/kmol
R_i = pore radius, m
$S_{o,\ N}$ = initial reaction surface, m^2/m^3; N, reaction surface for cycle N
t = time, s
$V^M_{CaO,CaCO3}$ = molar volumes, m^3/kmol
X = CaO molar conversion; N, relative to cycle N; K-D, transition between reaction regimes; r, residual CaO conversion
Z = ratio volume fraction after and before reaction

Greek letters

α = volume fraction of $CaCO_3$ invading a pore volume
$\beta = 2k_s a\rho(1-\varepsilon)/M_{CaO}bD_pS_o$
δ = decrease in pore radius upon carbonation, m
ε = porosity
$v_o(r)$ = pore radii distribution
ρ_{CaO} = CaO density, kg/m^3
$\tau = k_s(C_b - C_e)S_o t/(1-\varepsilon)$
$\Psi = 4\pi L_o(1-\varepsilon)/S_o^2$

Literature Cited

1. Metz B, Davidson O, de Coninck H, Loos M, Meyer L. *Special Report on Carbon Dioxide Capture and Storage, Intergovernmental Panel on Climate Change*. Cambridge: Cambridge University Press, 2005.
2. Shimizu T, Hirama T, Hosoda H, Kitano K, Inagaki M, Tejima K. A twin fluid-bed reactor for removal of CO_2 from combustion processes. *Chem Eng Res Des* 1999;77:62–68.
3. Abanades JC, Anthony EJ, Wang J, Oakey JE. Fluidized bed combustion systems integrating CO_2 capture with CaO. *Environ Sci Technol*. 2005;39:2861–2866.
4. Gupta H, Fan LS. Carbonation-calcination cycle using high reactivity calcium oxide for carbon dioxide separation from flue gas. *Ind Eng Chem Res*. 2002;41:4035–4042.
5. Anthony EJ. Solid looping cycles: a new technology for coal conversion. *Ind Eng Chem Res*. 2008;47:1747–1754.
6. Curran GP, Fink CE, Gorin E. Carbon dioxide-acceptor gasification process: studies of acceptor properties. *Adv Chem Ser*. 1967;69:141–165.
7. López-Ortiz A, Harrison DP. Hydrogen production using sorption-enhanced reaction. *Ind Eng Chem Res*. 2001;40:5102–5109.
8. Johnsen K, Grace JR, Elnashaie SSEH, Kolbeinsen L, Eriksen D. Modelling of sorption-enhanced steam reforming in a dual fluidized bubbling bed reactor. *Ind Eng Chem Res*. 2006;45:4133–4144.
9. Weimer T, Berger R, Hawthorne C, Abanades JC. Lime enhanced gasification of solid fuels: examination of a process for simultaneous hydrogen production and CO_2 capture. *Fuel*. 2008;87:1678–1686.
10. Florin NH, Harris AT. Mechanistic study of enhanced H_2 synthesis in biomass gasifyer with in-situ CO_2 capture using CaO. *AIChE J*. 2008;54:1096–1109.
11. Silaban A, Harrison DP. High-temperature capture of carbon dioxide: characteristics of the reversible reaction between CaO(s) and CO_2(g). *Chem Eng Commun*. 1995;137:177–190.
12. Barker R. The reversibility of the reaction $CaCO_3 = CaO + CO_2$. *J Appl Chem Biotechnol*. 1973;23:733–742.
13. Bathia SK, Perlmutter DD. Effect of the product layer on the kinetics of the CO_2-lime reaction. *AIChE J*. 1983;39:79–86.
14. Abanades JC, Alvarez D. Conversion limits in the reaction of CO_2 with lime. *Energy Fuels*. 2003;17:308–315.
15. Grasa GS, Abanades JC. CO_2 capture capacity of CaO in long series of carbonation/calcination cycles. *Ind Eng Chem Res*. 2006;45:8846–8851.
16. Alvarez D, Abanades JC. Determination of the critical product layer thickness in the reaction of CaO with CO_2. *Ind Eng Chem Res*. 2005;44:5608–5615.
17. Alvarez D, Abanades JC. Pore-size and shape effects on the recarbonation performance of calcium oxide submitted to repeated calcination/recarbonation cycles. *Energy Fuels*. 2005;19:270–278.
18. Lee DK. An apparent kinetic model for the carbonation of calcium oxide by carbon dioxide. *Chem Eng Sci*. 2004;100:71–77.
19. Sun P, Grace JR, Lim CJ, Anthony EJ. A discrete-pore-size-distribution-based gas-solid model and its application to the CaO + CO_2 reaction. *Chem Eng Sci*. 2008;63:57–70.
20. Stanmore BR, Gilot P. Review-calcination and carbonation of limestone during thermal cycling for CO_2 sequestration. *Fuel Process Technol*. 2005;86:1707–1743.
21. Bhatia SK, Perlmutter DD. A random pore model for fluid-solid reactions. I. Isothermal, kinetic control. *AIChE J*. 1980;26:379–386.
22. Bhatia SK, Perlmutter DD. A random pore model for fluid-solid reactions. II. Diffusion and transport effects. *AIChE J*. 1981;27:247–254.
23. Sun P, Grace JR, Lim JC, Anthony EJ. Determination of intrinsic rate constants of the CaO-CO_2 reaction. *Chem Eng Sci*. 2008;63:47–56.
24. Grasa GS, Abanades JC, Alonso M, González B. Reactivity of highly cycled particles of CaO in a carbonation/calcination loop. *Chem Eng J*. 2008;137:561–567.
25. Mess D, Sarofim FA, Loongwell JP. Product layer diffusion during the reaction of calcium oxide with carbon dioxide. *Energy Fuels*. 1999;13:999–1005.
26. Gavalas GR. A random capillary model with application to char gasification at chemically controlled rates. *AIChE J*. 1980;26:577–585.
27. Dennis JS, Hayhurst AN. The effect of CO_2 on the kinetics and extent of calcination of limestone and dolomite particles in fluidised beds. *Chem Eng Sci*. 1987;42:2361–2372.

Manuscript received Jun. 24, 2008, and revision received Oct. 3, 2008.